Simulating Energy Flow in Biomolecules: Application to Tuna Cytochrome *c*

Qiang Wang,* Chung F. Wong,* and Herschel Rabitz#
*Department of Physiology and Biophysics, Mount Sinai School of Medicine, New York, New York 10029-6574, and
#Department of Chemistry, Princeton University, Princeton, New Jersey 08574 USA

ABSTRACT By constructing a continuity equation of energy flow, one can utilize results from a molecular dynamics simulation to calculate the energy flux or flow in different parts of a biomolecule. Such calculations can yield useful insights into the pathways of energy flow in biomolecules. The method was first tested on a small system of a cluster of 13 argon atoms and then applied to the study of the pathways of energy flow after a tuna ferrocytochrome *c* molecule was oxidized. Initially, energy propagated faster along the direction perpendicular to the heme plane. This was due to an efficient through-bond mechanism, because the heme iron in cytochrome *c* was covalently bonded to a cysteine and a histidine. For the oxidation of cytochrome *c*, electrostatic interactions also facilitated a long-range through-space mechanism of energy flow. As a result, polar or charged groups that were further away from the oxidation site could receive energy earlier than nonpolar groups closer to the site. Another bridging mechanism facilitating efficient long-range responses to cytochrome *c* oxidation involved the coupling of far-off atoms with atoms that were nearer to, and interacted directly with, the oxidation site. The different characteristics of these energy transfer mechanisms defied a simple correlation between the time that the excess energy of the oxidation site first dissipated to an atom and the distance of the atom from the oxidation site. For tuna cytochrome *c*, all of the atoms of the protein had sensed the effects of the oxidation within ~40 fs. For the length scale of energy transfer considered in this study, the speed of the energy propagation in the protein was on the order of 10^5 m/s.

INTRODUCTION

Protein molecules are typically inhomogeneous and anisotropic. It is therefore expected that the efficiency of energy flow can vary from one part of a protein to another. An interesting issue to address is whether there are preferred pathways of energy flow, and whether one can modulate the pathways of energy flow and thus control the activity of a protein in a desired manner. In this study we have used cytochrome *c* as a model system for elucidating the mechanism of energy flow in protein molecules. The class of cytochrome *c* molecules contains heme-centered redox sites. When the heme of a cytochrome *c* molecule is oxidized or reduced after electron transfer, the energy deposited in the heme must be redistributed to its surroundings. To examine how this energy dissipates throughout the protein, we have calculated and analyzed the energy flow through each atom of the protein as a function of time.

To study energy flow through biomolecules, one can follow an approach developed by Schwieters and Rabitz (1994). These authors have adopted an approach of continuum mechanics (McQuarrie, 1976) to derive an equation for calculating energy flux in different parts of a molecule, using data generated from a molecular dynamics simulation. The calculated energy flux can be displayed concurrently with dynamic snapshots of the molecule to gain insights into the mode of energy flow occurring within the molecule. This method (the SR method) was previously applied to the study of energy flow within a 10-atom linear chain and a 3,4-dimethyl octane molecule (Schwieters and Rabitz, 1994).

This paper focuses on studying energy flow in a larger and more complex biomolecule, tuna cytochrome *c*. This study is useful because no detailed experimental or theoretical study on the mode of energy flow in proteins has yet been carried out. Energy dissipation on the molecular scale may be quite different from that on the macroscopic scale. The dissipation of energy during an earthquake, for example, may be viewed as a progressive, radial spread of energy from the epicenter. Locations near the epicenter feel the effects of the earthquake earlier than those further away from the epicenter. In studying energy flow in protein molecules, the length scale of interest is the dimension of the protein molecules. The length scale of protein molecules is comparable to the range of intramolecular interactions. Within this length scale, there may not be a direct correlation between the distance of an atom from a perturbed site of a protein and the delay time at which the atom starts to feel the effect of the perturbation. The study of energy flow inside the redox protein tuna cytochrome *c* can yield useful insights into the mechanism of energy flow occurring in the biomolecular length scale.

The next section summarizes key features of the SR method and derives expressions for calculating energy flow through different atoms of a protein molecule. The third section first describes the application of this method to the study of the energy flow in a small cluster of 13 argon atoms. It is easier to use a simpler system to illustrate the

Received for publication 7 October 1996 and in final form 31 March 1998.
Address reprint requests to Dr. Chung F. Wong, Department of Physiology and Biophysics, Mount Sinai School of Medicine, City University of New York, New York, NY 10029-6574. Tel.: 212-241-6533; Fax: 212-860-3369; E-mail: wong@msvax.mssm.edu.

0006-3495/98/07/60/10 $2.00

insights that can be obtained by this approach to studying energy flow within molecules. The application of this approach to studying energy flow in tuna ferrocytochrome *c* will then be described. The fourth section concludes.

METHOD

The SR method (Schwieters and Rabitz, 1994) gives the following expression for calculating the energy flux $\vec{J}(\vec{r},t)$ at time t and position $\vec{r}$ in a molecular system:

$$\vec{J}(\vec{r}, t) = -\frac{1}{4\pi}\left\{\sum_{i=1}^{N}\left[\frac{dP_i(t)}{dt} - S_i(t) + P_i(t)\frac{d}{dt}\right]\frac{(\vec{r} - \vec{r}_i(t))}{|\vec{r} - \vec{r}_i(t)|^3}\right\}. \quad (1)$$

where N is the number of atoms in the system, $S_i(t)$ is a source/sink term describing the energy flow between the system and its surroundings, and $dP_i(t)/dt$ is the time derivative of the energy $P_i(t)$ of atom i given by

$$P_i(t) = \frac{1}{2} m_i \left|\frac{d\vec{r}_i}{dt}\right|^2 + V_i. \quad (2)$$

The first term on the right-hand side of Eq. 2 is the kinetic energy, and the second term is the potential energy associated with atom i. In the simulations carried out in this work, no source/sink term was included, so that there was no interchange of energy between a simulated system and its surrounding. Energy terms in typical molecular mechanics force fields—such as the GROMOS force field (van Gunsteren and Berendsen, 1987) used in the cytochrome *c* simulations of this work—are usually composed of two-body, three-body, and four-body terms. To study energy flow through different atoms, one must introduce an energy partition scheme so that one can calculate the energy of each atom at any instant. A simple way to do this is to assume that the energy of each two-body term is shared equally between the two atoms involved in the energy term, the energy of each three-body term is shared equally among the three atoms involved in the energy term, etc. If this energy partition scheme is adopted, the total potential energy of a simulated system can be written as $V = \Sigma_i V_i$, in which V_i for each atom i can be assumed to take the form

$$V_i = \sum_{l=1}^{N_v} [\delta_{i,\alpha}\Gamma_l^{\alpha} + \delta_{i,\beta}\Gamma_l^{\beta} + \delta_{i,\gamma}\Gamma_l^{\gamma} + \delta_{i,\delta}\Gamma_l^{\delta}]v_l^{\alpha\beta\gamma\delta}(I_{l1}, I_{l2}, \ldots), \quad (3)$$

where N_v is the number of terms in the potential function that involve atom i. Each term v_l is expressed in terms of one or more internal coordinates (I_{l1}, I_{l2}, . . . etc.), which in turn depend on two or more atomic positions (r_α, r_β, r_γ, . . .), or directly in terms of atomic coordinates. The atomic indices α, β, γ, and δ depend implicitly on the index l. $\delta_{i,\alpha}$ is the Kronecker delta function, and Γ_l^{α} are energy partitioning weights. The sum of Γ_l^{α} is unity for each interaction term in the potential function. For the energy partition scheme described above, $\Gamma_l^{\alpha} = \Gamma_l^{\beta} = 1/2$ for two-body interactions, $\Gamma_l^{\alpha} = \Gamma_l^{\beta} = \Gamma_l^{\gamma} = 1/3$ for three-body interactions, and $\Gamma_l^{\alpha} = \Gamma_l^{\beta} = \Gamma_l^{\gamma} = \Gamma_l^{\delta} = 1/4$ for four-body interactions. The choice of these energy-partitioning weights corresponds to an equal distribution of the energy of each energy term to the atoms involved in the energy term. For example, if $v_1^{\alpha\beta\gamma\delta}$ represents a torsional energy term involving atoms α, β, γ, and δ, the energy associated with this term is split into four equal parts, with each of the four atoms sharing 1/4 of the torsional energy. If v_l represents the electrostatic interaction between two atomic partial charges, only two atoms, α and β, are involved in v_l, and each atom is allocated one-half of this electrostatic energy.

From Eq. 1, the energy flow through atom i at time t can be obtained by integrating the energy flux $\vec{J}(\vec{r},t)$ over a surface surrounding this atom, and the result is

$$EF_i(t) = -\frac{dP_i(t)}{dt}, \quad (4)$$

where $EF_i(t)$ is the energy flow through atom i. A positive $EF_i(t)$ suggests a net energy flow out of atom i, whereas a negative $EF_i(t)$ implies a net energy flow into atom i. Substituting Eq. 2 into Eq. 4 gives

$$EF_i(t) = -\vec{F}_i(t)\cdot\vec{v}_i(t) - \frac{dV_i(t)}{dt}. \quad (5)$$

On the right-hand side of Eq. 5, the first term originates from the kinetic energy and describes the kinetic energy flow at time t ($KEF_i(t)$); the second term arises from the potential energy and is referred to as the potential energy flow ($VEF_i(t)$). They are expressed, respectively, as

$$KEF_i(t) = -\vec{F}_i(t)\cdot\vec{v}_i(t), \quad (6)$$

and

$$VEF_i(t) = -\frac{dV_i(t)}{dt}. \quad (7)$$

Because the source term $S_i(t)$ of Eq. 1 was taken to be zero (i.e., $S_i(t) = 0$) in this work, conservative systems were simulated such that the following relations held:

$$\sum_i^N KEF_i(t) = -\sum_i^N VEF_i(t), \quad (8)$$

and

$$\sum_i^N EF_i(t) = 0. \quad (9)$$

To simulate a small cluster of 13 argon atoms, the starting structure was constructed by arranging the argon atoms at the corners and center of an icosahedron as shown in Fig. 1. Two argon atoms in this system interacted through a Len-

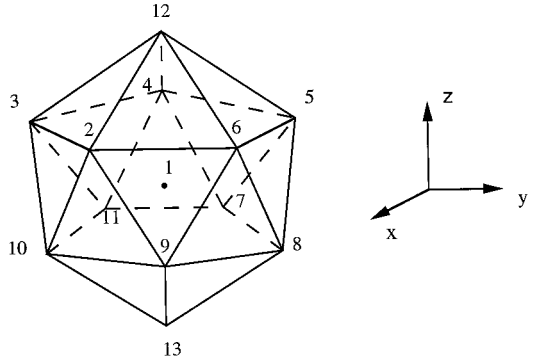

FIGURE 1 The equilibrium icosahedral structure of Ar_{13}.

nard-Jones potential of the form

$$V_{ij}(r) = 4\epsilon\left[\left(\frac{\sigma}{r_{ij}}\right)^{12} - \left(\frac{\sigma}{r_{ij}}\right)^{6}\right]. \quad (10)$$

A molecular dynamics simulation of the argon cluster was carried out using a Verlet's algorithm with a time step of $0.001t_A$, where $t_A = (m\sigma^2/\epsilon)^{0.5} = 2.2$ ps for argon. The initial velocities were nonzero ($= 1.0(r_0/t_A)$, where $r_0 = 2^{1/6}\sigma$ and $\sigma = 0.34$ nm) only for the center atom in the x direction.

The tuna ferrocytochrome *c* simulation, similar to the one described by Wong et al. (1993), was carried out by using the GROMOS force field (van Gunsteren and Berendsen, 1987) that contains a sum of Coulombic, Lennard-Jones, bond-stretching, angle-bending, torsional, proper dihedral, and improper dihedral terms. The simulation was performed by starting with the x-ray structure of tuna ferrocytochrome *c* determined by Takano and Dickerson (1981). Polar hydrogens were added and nonpolar hydrogens were accounted for implicitly by the extended atom representation (McCammon and Harvey, 1987). A cytochrome *c* molecule was put in a truncated octahedral box filled with SPC/E water molecules (Berendsen et al., 1987). Water molecules with oxygens located 2.3 Å or less from a protein heavy atom were deleted. The system contained 3128 water molecules, and the distance between the edge of the box and the closest protein atom was at least 10 Å. A cutoff of 9 Å was used for the nonbonded interactions, and periodic boundary conditions were used in the simulation. Equilibration of the system was then carried out by first performing 100 steps of steepest descent energy minimization to relieve bad contacts. A molecular dynamics simulation was then carried out with the protein atoms held almost stationary by applying harmonic constraining potentials to the protein atoms. Maxwellian velocities were reassigned every 0.5 ps during this period of the simulation. The SHAKE algorithm (Ryckaert et al., 1977) was used to constrain all of the bond lengths, and a time step of 2 fs was used. After 5 ps of equilibration of water molecules, the protein atoms were also allowed to relax by removing the harmonic restraints, and the whole system was allowed to equilibrate for an additional 10 ps with Maxwellian velocity reassignments at 0.5-ps intervals. The system was subsequently coupled to a temperature bath with a relaxation time of 0.1 ps (Berendsen et al., 1984). The equilibration was continued for 5 more ps before velocity reassignments were stopped. The simulation was then continued for more than 300 ps.

To carry out the energy flow study, four phase points (at 150 ps, 200 ps, 250 ps, and 300 ps) were selected from the above molecular dynamics simulation of tuna ferrocytochrome *c*. Two simulations were then carried out, starting from each one of these four phase points. One was still on the reduced form of the molecule, except that a small time step of 0.5 fs was now used to follow the fast energy dissipation that could occur within a cytochrome *c* molecule. The other was on the oxidized form of the molecule, using the same simulation conditions as the reduced form. For the simulation of the oxidized form, the heme group was switched from the reduced to the oxidized form instantaneously by changing the force field parameters from the reduced to the oxidized form. In this work we assumed that in going from the reduced to the oxidized form of cytochrome *c*, an extra unit positive charge was distributed uniformly on the heme iron and the six atoms covalently bonded to it. Both simulations were carried out for 200 time steps, or 100 fs, and no heat bath was used in the simulations. The energy flow associated with each atom was calculated every two time steps for the reduced and the oxidized forms of the cytochrome *c* molecule. The energies (resulting from the oxidation of the protein) that needed to be dissipated from the oxidation site of the protein were 240 kJ/mol, 150 kJ/mol, 220 kJ/mol, and 170 kJ/mol, respectively, for the sets of simulations originating from the 150-ps, 200-ps, 250-ps, and 300-ps snapshots of the ferrocytochrome *c* simulation.

RESULTS AND DISCUSSION

Ar_{13}

The dynamics simulation of the argon cluster was carried out for 22 ps, and the last 4 ps was used for analysis. Fig. 2 shows the time evolution of the total and potential energies. The total energy was conserved to within 0.01% during the simulation. The potential energy oscillated around 43.97 kJ/mol and exchanged with the kinetic energy from time to time. This is consistent with the requirements of Eqs. 8 and 9 for a conservative system. The time integration of the KEF and VEF should also be zero periodically, when the total kinetic energy or the potential energy returned to its value at the starting time point. That this condition was satisfied is shown in Fig. 3.

Although one can gain insights into how energy propagates within a system by monitoring the energy change of each atom as a function of time, it is more sensitive to monitor the energy flow associated with each atom. To illustrate this point, we selected a snapshot from the molecular dynamics trajectory of the argon cluster, increased the

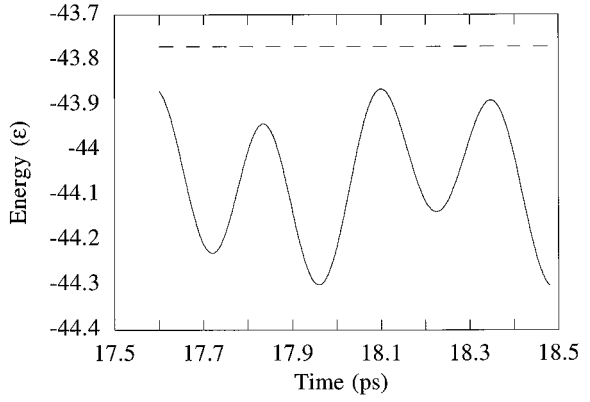

FIGURE 2 Time evolution of the total (– – –) and potential (——) energies of Ar_{13}.

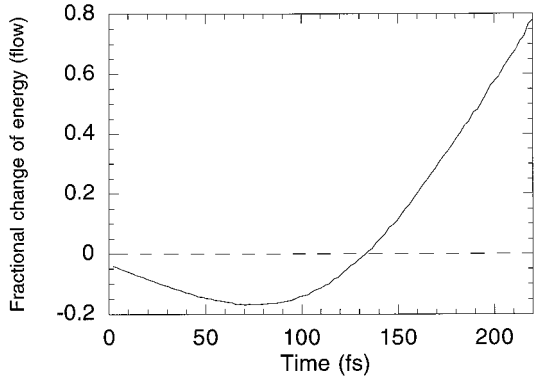

FIGURE 4 Comparison of the fractional change of the total energy (– – –) and the energy flow (——) for atom 12 of Ar_{13} during the first 100 steps after the center atom (atom 1) of the argon cluster was disturbed.

x component of the velocity of the center atom in the cluster by 50% to 1.5 (r_0/t_A), and calculated the fractional change of the energy and the energy flow resulting from this velocity perturbation as a function of time. (Note that this increase in velocity corresponded to dumping an energy of 0.5 kJ/mol into the central atom of the cluster, and this excess energy was gradually distributed to the rest of the cluster as the system restored equilibrium.) One can see from Fig. 4 that the fractional change of the energy of the 12th atom is much smaller than the fractional change of its energy flow. Energy flow is thus a more sensitive quantity than energy for revealing energy relaxation pathways in complex molecules.

To determine whether there was any correlation in the energy flow among the atoms in the argon cluster, we calculated the correlation matrix of energy flow. The matrix elements of the correlation matrix had the form

$$C_{ij} = \langle (EF_i - \langle EF_i \rangle)(EF_j - \langle EF_j \rangle) \rangle / \sqrt{\langle (EF_i - \langle EF_i \rangle)^2 \rangle \langle (EF_j - \langle EF_j \rangle)^2 \rangle},$$

where i and j label atoms i and j. By diagonalizing this correlation matrix, one could identify the most important modes for energy transfer in this cluster. The two most important modes have the following characteristics. The eigenvector corresponding to the mode with the largest eigenvalue of the energy flow correlation matrix has a zero component for the central atom, 0.3 for atoms 2, 3, 4, 5, 6, and 12, and −0.3 for atoms 7, 8, 9, 10, 11, and 13. This mode describes the energy flow into atoms 2, 3, 4, 5, 6, and 12 from atoms 7, 8, 9, 10, 11, and 13 or vice versa, and the central atom is not involved in this mode (Fig. 5). The eigenvector associated with the second most correlated mode has components of 0.2 for atoms 2–13 and −0.6 for atom 1, the central atom. This mode of energy flow describes the exchange of energy between the central atom and the surrounding atoms (Fig. 5). Hence efficient pathways of energy flow in the argon cluster appear to be facilitated by collective motions of the argon cluster. Other mechanisms of energy transfer, such as the sequential transfer of energy from one atom to another, are less efficient for this cluster at the energy considered in this study.

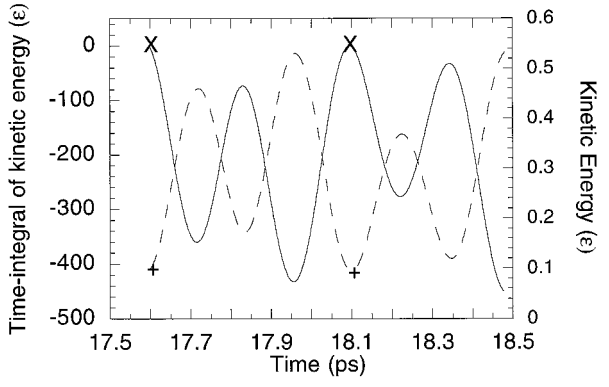

FIGURE 3 Time evolution of the kinetic energy (– – –) of Ar_{13} and the time integral of the kinetic energy flow (——). In going from a point + to the next one + having the same kinetic energy, the time integral of the kinetic energy is also unchanged (the two points marked ×).

Cytochrome *c*

The mechanism of energy transfer in cytochrome *c* may be more complex than that of the 13-atom argon cluster be-

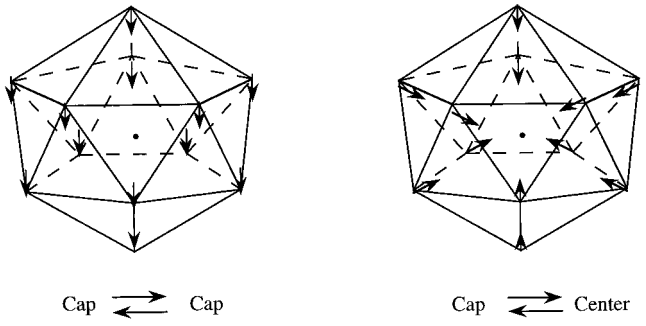

FIGURE 5 The two major collective modes of energy flow in Ar_{13}. Mode 1 is the cap-to-cap mode. Mode 2 is the caps-to-center mode.

cause of the larger size of the protein molecule and the presence of both short-range and long-range interactions. We have studied the energy flow patterns of this protein after its oxidation by carrying out four sets of simulations for the oxidized and reduced forms of cytochrome *c* described under Method. Using Eq. 4, the energy flow (EF_i) for each atom i as a function of time for both oxidation states of the protein could be calculated for each set of these simulations. Taking the difference in the energy flow between the oxidized ($EFO_i(t)$) and the reduced ($EF_i(t)$) forms ($EFO_i(t) - EF_i(t)$) as a function of time, one could observe (Fig. 6) a delay time after which an atom started feeling the effects of the oxidation of the heme. This delay time varied from one atom to another. Some atoms responded to the perturbation of the heme group more rapidly than others. If one defined the delay time of atom i to be the time at which $EFO_i(t) - EF_i(t)$ first changed by 0.5 kJ/mol/ps or more than the corresponding value in the previous time step, one could calculate and compare the delay times of all of the atoms in the protein molecule. The calculation of these delay times can help us to graphically visualize the dissipation of energy from the oxidation site of a cytochrome *c* molecule to the rest of the protein. In Fig. 7 *A*, the atoms responding within 1 fs after oxidation are shown as darker than those atoms that took longer to respond. One can see that energy dissipated preferentially along the axial direction of the heme. The efficient energy transfer along the axial direction was facilitated by a combination of through-bond and through-space mechanisms. The heme of tuna cytochrome *c* has two axial ligands, His^{18} and Met^{80}. These two ligands are covalently bonded to the iron of the heme and help to dissipate energy away from the heme iron through the iron-ligand bonds. Because of this through-bond mechanism, many atoms from residues 13 to 20 and from 76 to 82 responded quickly to the oxidation. On the other hand, electrostatic interactions provided an efficient mechanism for long-range energy transfer. As a result of these interactions, some polar atoms far away from the heme responded within 1 fs after oxidation. An example is the hydroyxl group of Tyr^{67}. Many atoms of peptide bonds also sensed the oxidation quickly because they are polar. Similarly, it is not surprising to see within 1 fs the response of the charged carboxylate groups and the silence of the nonpolar hydrocarbon chains of both propionates, even though the hydrocarbon chains are closer to the heme iron. The side chain of Asp^{52}, which is hydrogen-bonded to one of the propionates, also felt the effect of the oxidation within 1 fs. Fig. 7, *B* and *C*, shows the atoms that had responded to the heme oxidation after 5 fs and 10 fs of oxidation. These results further demonstrate the more rapid response of polar and charged groups to the oxidation than nonpolar groups. In view of these results, the selective replacements of charged or polar groups with nonpolar ones, or vice versa, may provide a strategy for redirecting energy flow in biomolecules. Because polar peptide groups facilitate energy transfer after a redox reaction has taken place, their modifications can also alter the pathways of energy flow in a desired manner. In addition, one can make or break bonds to redirect energy flow within a biomolecule.

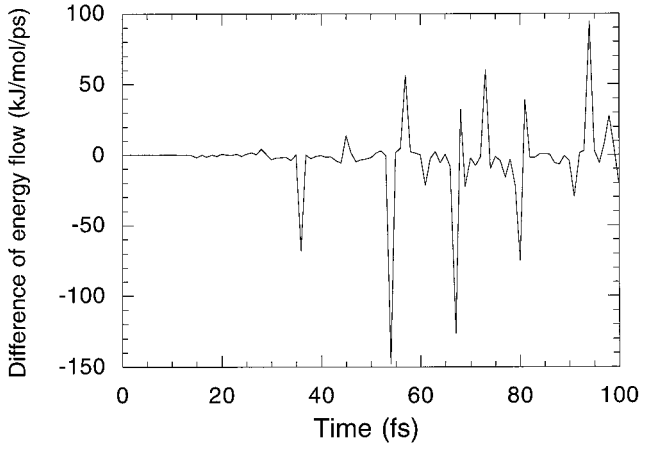

FIGURE 6 Time evolution of the difference of the energy flow after and before oxidation of the heme group of the amino hydrogen of GLY1.

For the case starting from the 200-ps phase point, the inverses of the delay times of the protein atoms are shown in Fig. 8. The data were normalized so that the maximum value was 1, corresponding to atoms having the fastest time of response to the oxidation of the heme group. Atoms that had small values of the inverse of the decay times took longer to respond to the oxidation of the heme. It is clear from Fig. 8 that there were atoms that responded very quickly to the oxidation, but there were also atoms that took a significantly longer time to feel the effects of the oxidation. The delay times varied from 1 fs to 40 fs. Considering the length scale of the protein, the speed of energy dissipation was on the order of 10^5 m/s.

We have also examined whether the qualitative insights provided by the above delay times were sensitive to the choice of initial conditions, by repeating the delay time analysis and using trajectories of the oxidized and reduced forms of the protein originating from other snapshots (150 ps, 250 ps, and 300 ps) of the ferrocytochrome *c* simulation. Although there were some minor quantitative differences, the results obtained by using different starting points were qualitatively similar. The atoms that responded within 1 fs of the oxidation are shown in Table 1. As discussed earlier, the propionate group of the pyrrole ring A ($\sim$7.5 Å from the Fe) of the heme was among the group of atoms that responded quickly to the oxidation. This propionate group was also among the groups of atoms of the protein that were observed to show larger structural changes due to the alternation of the oxidation state of the protein (Berghuis and Brayer, 1992).

We have also examined whether there is a correlation between the response (or delay) time of an atom to the oxidation of the protein and the distance of the atom from the heme iron (Fig. 9). It is clear from Fig. 9 that the delay time of an atom was not simply determined by the distance of the atom to the heme iron. Although many atoms close to

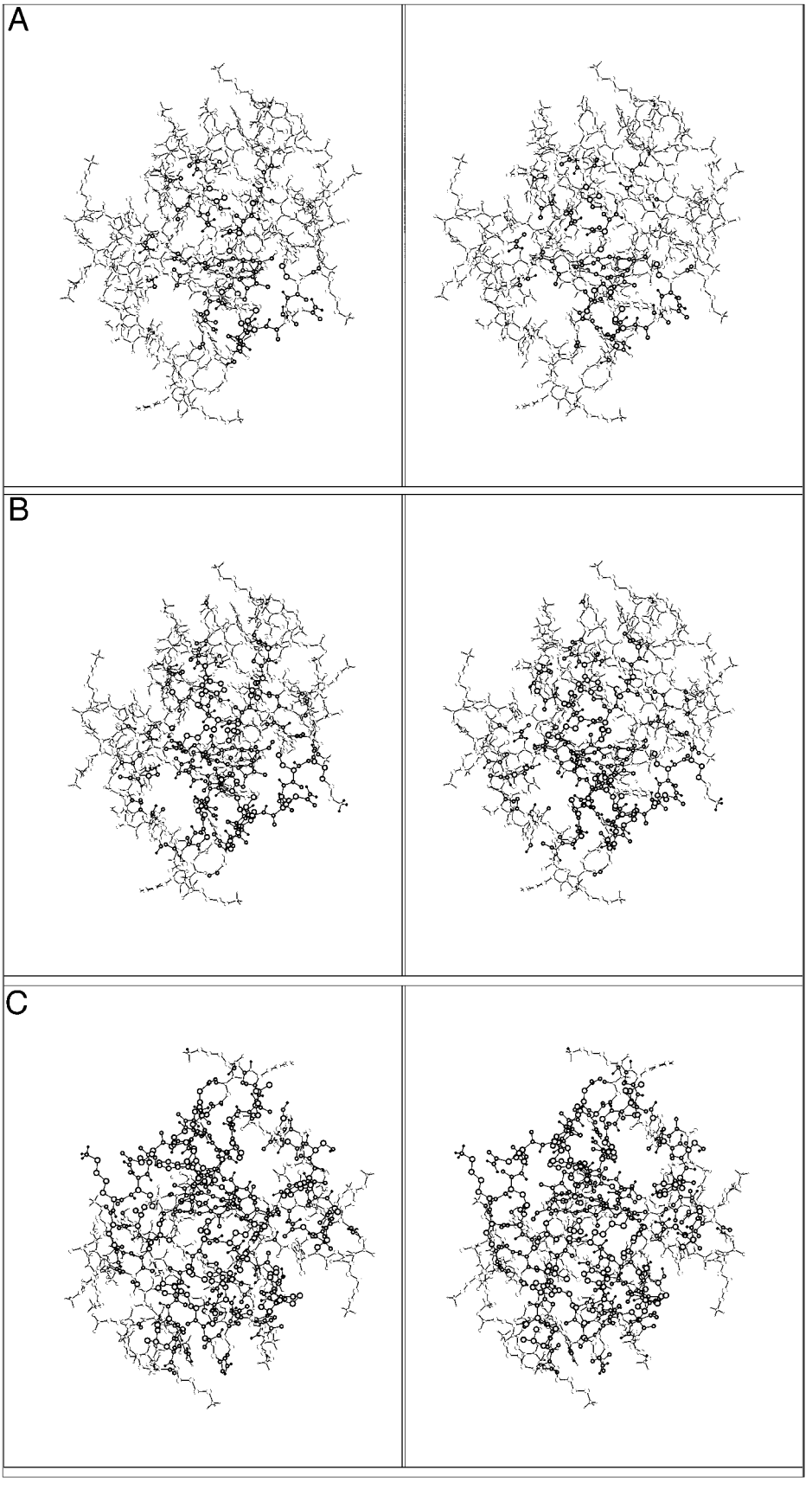

FIGURE 7 (*A*) Darker atoms are those that responded within 1 fs after oxidation of the heme. (*B*) Darker atoms are those that responded within 5 fs after oxidation of the heme. (*C*) Darker atoms are those that responded within 10 fs after oxidation of the heme.

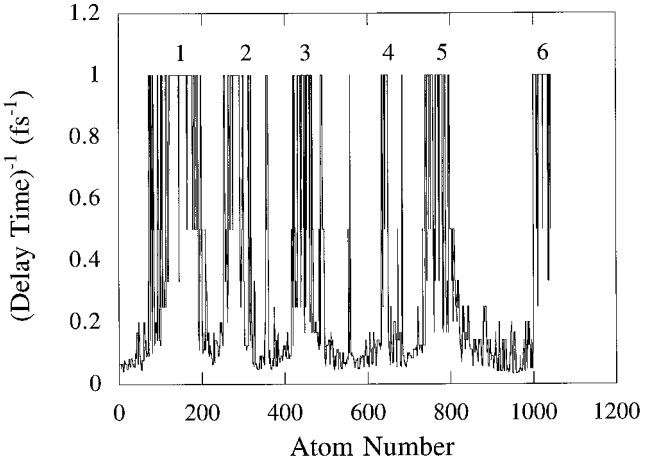

FIGURE 8 Distribution of delay times in cytochrome *c*.

the heme iron had short delay times, some atoms that were far away from the heme iron could also respond quickly to the oxidation. This is not surprising, because the length scale of interest here is the dimension of the protein (having a radius of 20 Å or so); this length scale is comparable to the range in which intramolecular interactions are significant. Because of the different characteristics of different atoms in the protein, an atom further away from the heme iron may interact more strongly with the heme iron than an atom closer to the heme iron. For example, the atom further away from the heme iron may be charged, whereas the atom closer to the heme iron may carry a negligible partial charge. Because of the long-range effects of electrostatic interactions and other indirect mechanisms discussed earlier and below, energy dissipation on the molecular scale may not appear as smooth and gradual as the propagation of a wave resulting from the dropping of a stone into a pond, for example.

To further understand how energy is transmitted from the oxidized heme atoms to other atoms in the protein, it is useful to reexamine Eq. 5 in finer detail for calculation of the energy flow into or out of an atom. Equation 5 can be written in another equivalent form:

$$\mathrm{EF}_i(t) = \sum_j \vec{v}_i(t) \cdot \nabla_i V_j - \sum_j \vec{v}_j(t) \cdot \nabla_j V_i, \qquad (11)$$

where $\nabla_i V_j$ is the gradient of the potential energy of atom j relative to the coordinates of atom i, and $\vec{v}_j(t)$ is the velocity of atom i. For any atom i, only those atoms j that interact with i (i.e., not both $\nabla_i V_j$ and $\nabla_j V_i$ are zeros) can give nonzero contributions to $\mathrm{EF}_i(t)$. We call these atoms j "nonzero contribution atoms" to the energy flux at atom i. Among these nonzero contribution atoms to atom i, some may change their energy flow contributions to atom i after oxidation occurs. These atoms are further labeled as "oxidation-sensitive atoms." Atom j can feel the oxidation effect because it is interacting directly with the oxidation site (i.e., the interaction energy between j and the oxidation site is nonnegligible), or it can interact indirectly with the oxidation site through other atoms.

TABLE 1 Atoms that respond to the oxidation effect of the heme within 1 fs after the oxidation of tuna ferrocytochrome *c*

Column 1		Column 5		Column 6	
O(10.6)	9Thr	C(13.8)	76Pro	Fe(0.0)	104Heme
C(8.5)	13Lysh	O(13.2)	76Pro	NA(2.1)	104Heme
C(8.2)	13Lysh	C(11.9)	77Gly	NB(2.1)	104Heme
CB(6.6)	14Cys	O(11.7)	77Gly	NC(2.1)	104Heme
SG(6.7)	14Cys	N(11.1)	78Thr	ND(2.1)	104Heme
C(7.0)	14Cys	H(11.7)	78Thr	C1A(3.1)	104Heme
O(6.4)	14Cys	CB(9.3)	78Thr	C2A(4.2)	104Heme
N(8.2)	15Ala	OG1(8.0)	78Thr	C4A(3.0)	104Heme
H(8.9)	15Ala	HG1(7.8)	78Thr	CGA(6.8)	104Heme
C(9.0)	15Ala	C(9.0)	78Thr	O1A(7.6)	104Heme
O(9.4)	15Ala	N(8.7)	79Lysh	O2A(7.4)	104Heme
N(9.1)	16Gln	H(8.5)	79Lysh	CHB(3.2)	104Heme
H(9.3)	16Gln	C(7.8)	79Lysh	C1B(3.2)	104Heme
CD(12.2)	16Gln	O(8.3)	79Lysh	C2B(4.3)	104Heme
OE1(12.9)	16Gln	N(6.7)	80Met	C3B(4.1)	104Heme
NE2(12.6)	16Gln	H(6.5)	80Met	C4B(3.0)	104Heme
HE21(13.5)	16Gln	CA(5.8)	80Met	CAB(5.5)	104Heme
HE22(12.1)	16Gln	SD(2.3)	80Met	CHC(3.5)	104Heme
C(8.9)	16Gln	C(6.7)	80Met	C1C(3.0)	104Heme
O(9.7)	16Gln	O(7.6)	80Met	C2C(4.3)	104Heme
N(7.6)	17Cys	N(7.0)	81Ile	C4C(3.2)	104Heme
H(7.0)	17Cys	H(6.5)	81Ile	CMC(5.6)	104Heme
CA(6.9)	17Cys	CA(8.1)	81Ile	CHD(3.4)	104Heme
CB(5.9)	17Cys	N(8.7)	82Phe	C4D(3.0)	104Heme
SG(6.7)	17Cys	H(8.9)	82Phe	CBD(6.7)	104Heme
C(6.4)	17Cys	C(10.5)	82Phe	CGD(7.8)	104Heme
O(6.7)	17Cys	N(11.6)	83Ala	O2D(7.7)	104Heme
N(5.8)	18His				
H(5.6)	18His				
CA(6.0)	18His				
ND(4.0)	18His				
HD(4.8)	18His				
CD2(2.9)	18His				
CE1(2.9)	18His				
NE2(2.0)	18His				
C(7.5)	18His				
N(8.4)	19Thr				
H(8.3)	19Thr				
CA(9.8)	19Thr				
OG1(10.3)	19Thr				
HG1(10.9)	19Thr				
O(10.3)	19Thr				
N(11.8)	20Val				
H(11.9)	20Val				
C(14.0)	20Val				

Atoms in columns 1, 5, and 6 of Fig. 7 are listed. Distances (in Å) of each atom from the heme iron are in parentheses.

The difference in the energy flow between the oxidized and reduced forms of cytochrome *c* for atom i at time *t* can be obtained as

$$\begin{aligned}\mathrm{DEF}_i(t) &= \mathrm{EF}_i^{\mathrm{A}}(t) - \mathrm{EF}_i^{\mathrm{B}}(t) \\ &= \sum_j \vec{v}_i^{\mathrm{A}}(t) \cdot \nabla_i V_j^{\mathrm{A}} - \sum_j \vec{v}_j^{\mathrm{A}}(t) \cdot \nabla_j V_i^{\mathrm{A}} \\ &\quad - \sum_j \vec{v}_i^{\mathrm{B}}(t) \cdot \nabla_i V_j^{\mathrm{B}} + \sum_j \vec{v}_j^{\mathrm{B}}(t) \cdot \nabla_j V_i^{\mathrm{B}}.\end{aligned} \qquad (12)$$

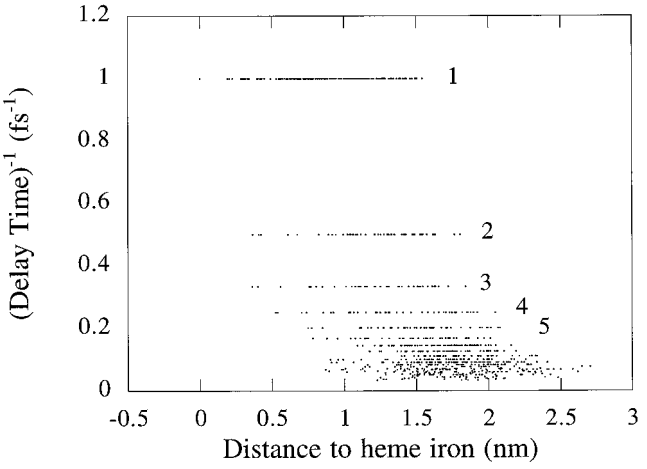

FIGURE 9 The correlation of the delay time of an atom to the distance of the atom from the oxidation site of cytochrome *c*.

where A stands for after and B stands for before oxidation. Two special cases of Eq. 12 were found to occur in the cytochrome *c* simulations:

1. $\nabla_i V_j^A = \nabla_i V_j^B$ and $\nabla_j V_i^A = \nabla_j V_i^B$, so that

$$\mathrm{DEF}_i(t) = \sum_j (\vec{v}_i^A - \vec{v}_i^B) \cdot \nabla_i V_j^A - \sum_j (\vec{v}_j^A - \vec{v}_j^B) \cdot \nabla_j V_i^A. \quad (13)$$

2. $\vec{v}_i^A = \vec{v}_i^B$ and $\vec{v}_j^A = \vec{v}_j^B$, so that

$$\mathrm{DEF}_i(t) = \sum_j \vec{v}_i^A \cdot (\nabla_i V_j^A - \nabla_i V_j^B) - \sum_j \vec{v}_j^A \cdot (\nabla_j V_i^A - \nabla_j V_i^B). \quad (14)$$

Case 1 was observed for the amide hydrogen (H-TRP33) of TRP33. In the energy flow calculations starting from the 150-ps snapshots of the ferrocytochrome *c* simulation, the delay time of atom H-TRP33 was found to be very fast (1 fs), even though H-TRP33 was ~12 Å away from the heme iron. It had a total of 142 nonzero contribution atoms, including both protein and solvent atoms. However, only 22 of these nonzero contribution atoms were oxidation-sensitive atoms. Table 2 lists the oxidation-sensitive atoms of H-TRP33 1 fs after oxidation of the heme. These oxidation-sensitive atoms did not change their interactions with H-TRP33 when the protein was oxidized; only their velocities were perturbed by the oxidation. Although the direct interaction potential between H-TRP33 and a perturbed atom near the oxidation site was negligible, H-TRP33 responded quickly to the oxidation by interacting with atoms such as

TABLE 2 The oxidation-sensitive protein atoms of the amide hydrogen of TRP33

Residue	Atom	EF	DEF
18His	C(7.5)	13.100	0.014
18His	O(7.9)	−0.313	0.013
19Thr	N(8.4)	−0.897	−0.021
19Thr	H(8.3)	22.302	0.059
19Thr	O(10.3)	59.659	0.023
20Val	N(11.8)	104.426	0.009
30Pro	C(8.4)	92.484	−0.015
30Pro	O(8.0)	−86.568	0.012
31Asn	N(9.3)	−94.208	−0.024
31Asn	H(9.8)	103.129	0.053
31Asn	CG(12.1)	69.236	0.042
31Asn	C(9.3)	596.436	0.071
32Leu	H(9.5)	219.605	0.686
104Heme	CGA(6.8)	91.104	−0.026
104Heme	O1A(7.6)	−199.781	0.036
104Heme	O2A(7.4)	−280.447	−0.016

Distances (in Å) of each atom from the heme iron are in parentheses. EF and DEF are in kJ/mol.

TABLE 3 The oxidation-sensitive protein atoms of the heme iron

Residue	Atom	EF	DEF
14Cys	CB(6.6)	−1.530	−0.548
14Cys	SG(6.7)	−27.508	−9.674
14Cys	C(7.0)	10.581	3.571
14Cys	O(6.4)	−12.403	−4.542
17Cys	N(7.6)	11.595	4.089
17Cys	H(7.0)	15.401	4.254
17Cys	CB(5.9)	3.623	1.237
17Cys	SG(6.7)	4.937	1.643
17Cys	C(6.4)	−20.876	−7.584
17Cys	O(6.7)	21.596	7.379
18His	N(5.8)	20.402	6.989
18His	H(5.6)	41.544	10.542
18His	HD1(4.8)	57.482	18.468
18His	CD2(2.9)	1.486	−0.120
18His	CE1(2.9)	18.312	−0.204
18His	NE2(2.0)	61.395	0.068
18His	C(7.5)	−7.362	−2.651
18His	O(7.9)	2.327	0.789
67Tyr	CZ(6.5)	−1.283	−0.303
67Tyr	OH(6.0)	−3.630	−1.872
67Tyr	HH(6.6)	25.710	7.488
80Met	N(6.7)	−3.774	−1.392
80Met	H(6.5)	−43.024	−16.910
80Met	CG(3.6)	74.929	−0.056
80Met	SD(2.3)	76.873	−0.153
80Met	CE(3.5)	6.718	−0.010
80Met	C(6.7)	14.355	4.660
80Met	O(7.6)	−9.597	−3.607
81Ile	N(7.0)	−19.320	−6.853
81Ile	H(6.5)	19.831	5.286
81Ile	C(8.1)	20.955	7.267
81Ile	O(7.5)	−9.046	−3.291
104Heme	NA(2.1)	10.193	0.281
104Heme	NB(2.1)	763.624	−0.964
104Heme	NC(2.1)	−570.263	−0.521
104Heme	ND(2.1)	48.870	0.122
104Heme	C1A(3.1)	−32.095	−0.037
104Heme	C4A(3.0)	−0.238	−0.627
104Heme	CGA(6.8)	−9.327	−3.287
104Heme	O1A(7.6)	1.384	0.279
104Heme	O2A(7.4)	45.974	15.841
104Heme	C1B(3.2)	−29.189	0.683
104Heme	C4B(3.0)	111.939	−0.139
104Heme	C1C(3.0)	38.254	−0.056
104Heme	C4C(3.2)	−61.868	−0.071
104Heme	C1D(3.2)	−118.374	0.064
104Heme	C4D(3.0)	91.025	0.143

Distances (in Å) of each atom from the heme iron are in parentheses.

TABLE 4 The bonding and nonbonding oxidation-sensitive atoms of the heme iron (250 ps)

	Residue	Atom	EF	DEF
Bonding	18His	CD2(2.9)	−27.488	−0.089
	18His	CE1(2.9)	−3.417	0.394
	18His	NE2(2.0)	50.660	0.194
	80Met	CG(3.6)	6.420	−0.233
	80Met	SD(2.3)	−142.878	−0.005
	80Met	CE(3.5)	−237.583	0.564
	104Heme	NA(2.1)	−469.242	−5.246
	104Heme	NB(2.1)	19.854	−0.596
	104Heme	NC(2.1)	−26.582	−0.402
	104Heme	ND(2.1)	17.951	0.994
	104Heme	C1A(3.1)	−522.921	−0.408
	104Heme	C4A(3.0)	−42.451	−0.271
	104Heme	C1B(3.2)	−59.676	−0.780
	104Heme	C4B(3.0)	−47.298	−0.373
	104Heme	C1C(3.0)	48.946	0.423
	104Heme	C4C(3.2)	−41.397	−0.718
	104Heme	C1D(3.2)	−75.248	0.115
	104Heme	C4D(3.0)	60.164	0.444
Nonbonding	14Cys	CB(6.6)	−2.451	−0.929
	14Cys	SG(6.7)	−7.155	−2.727
	14Cys	C(7.0)	−12.768	−4.382
	14Cys	O(6.4)	29.681	10.058
	17Cys	N(7.6)	1.350	0.412
	17Cys	H(7.0)	−12.024	−4.748
	17Cys	CB(5.9)	3.731	1.249
	17Cys	SG(6.7)	−17.953	−6.606
	17Cys	C(6.4)	39.347	13.685
	17Cys	O(6.7)	−5.769	−2.129
	18His	N(5.8)	−15.195	−5.415
	18His	H(5.6)	20.450	4.919
	18His	HD1(4.8)	0.736	−0.061
	67Tyr	CZ(6.5)	−0.603	−0.222
	67Tyr	OH(6.0)	14.081	4.517
	67Tyr	HH(6.6)	−71.899	−29.442
	79Lysh	C(7.8)	−16.916	−5.884
	79Lysh	O(8.3)	17.764	6.091
	80Met	N(6.7)	25.935	9.005
	80Met	H(6.5)	−20.083	−9.942
	80Met	C(6.7)	−42.925	−14.922
	80Met	O(7.6)	21.958	7.673
	81Ile	N(7.0)	23.490	8.085
	81Ile	H(6.5)	−17.988	−7.485
	104Heme	CGD(7.8)	3.980	1.310
	104Heme	O1D(8.8)	−30.850	−10.876
	104Heme	O2D(7.7)	−7.464	−2.757

Distances (in Å) of each atom from the heme iron are in parentheses. EF and DEF are in kJ/mol.

TABLE 5 The bonding and nonbonding oxidation-sensitive atoms of the heme iron (150 ps)

	Residue	Atom	EF	DEF
Bonding	18His	CD2(2.9)	1.486	−0.120
	18His	CE1(2.9)	18.312	−0.204
	18His	NE2(2.0)	61.395	0.068
	80Met	CG(3.6)	74.929	−0.056
	80Met	SD(2.3)	76.873	−0.153
	80Met	CE(3.5)	6.718	−0.010
	104Heme	NA(2.1)	10.193	0.281
	104Heme	NB(2.1)	763.624	−0.964
	104Heme	NC(2.1)	−570.263	−0.521
	104Heme	ND(2.1)	48.870	0.122
	104Heme	C1A(3.1)	−32.095	−0.037
	104Heme	C4A(3.0)	−0.238	−0.627
	104Heme	C1B(3.2)	−29.189	0.683
	104Heme	C4B(3.0)	111.939	−0.139
	104Heme	C1C(3.0)	38.254	−0.056
	104Heme	C4C(3.2)	−61.868	−0.071
	104Heme	C1D(3.2)	−118.374	0.064
	104Heme	C4D(3.0)	91.025	0.143
Nonbonding	14Cys	CB(6.6)	−1.530	−0.548
	14Cys	SG(6.7)	−27.508	−9.674
	14Cys	C(7.0)	10.581	3.571
	14Cys	O(6.4)	−12.403	−4.542
	17Cys	N(7.6)	11.595	4.089
	17Cys	H(7.0)	15.401	4.254
	17Cys	CB(5.9)	3.623	1.237
	17Cys	SG(6.7)	4.937	1.643
	17Cys	C(6.4)	−20.876	−7.584
	17Cys	O(6.7)	21.596	7.379
	18His	N(5.8)	20.402	6.989
	18His	H(5.6)	41.544	10.542
	18His	HD1(4.8)	57.482	18.468
	18His	C(7.5)	−7.362	−2.651
	18His	O(7.9)	2.327	0.789
	67Tyr	CZ(6.5)	−1.283	−0.303
	67Tyr	OH(6.0)	−3.630	−1.872
	67Tyr	HH(6.7)	25.710	7.488
	80Met	N(6.7)	−3.774	−1.392
	80Met	H(6.5)	−43.024	−16.910
	80Met	C(6.7)	14.355	4.660
	80Met	O(7.6)	−9.597	−3.607
	81Ile	N(7.0)	−19.320	−6.853
	81Ile	H(6.5)	19.831	5.286
	81Ile	C(8.1)	20.955	7.267
	81Ile	O(7.5)	−9.046	−3.291
	104Heme	CGA(6.8)	−9.327	−3.287
	104Heme	O1A(7.6)	1.384	0.279
	104Heme	O2A(7.4)	45.974	15.841

Distances (in Å) of each atom from the heme iron are in parentheses. EF and DEF are in kJ/mol.

the amide hydrogen of LEU32 that interacted directly with the epsilon nitrogen of HIS18 that was covalently bonded to the heme iron.

Case 2 was found for the heme iron in the same simulation. In this case, the oxidation-sensitive atoms of the reduced and the oxidized forms of cytochrome *c* differed in their interactions with the heme iron, but their velocities in the two forms of cytochrome *c* were quite similar at the delay time. Table 3 shows the oxidation-sensitive atoms of the heme iron. In contrast to the previous case 1 example, all of the nonzero contribution atoms were also oxidation-sensitive atoms in this case. Most of these atoms were relatively close to the heme iron. However, there were also atoms that were close to the heme iron, but were not nonzero contribution atoms of the heme iron. This observation further illustrates that there is no simple correlation between the delay time of an atom and its distance from the oxidation site of the protein.

One could also analyze the contributions of the bonding (two-body stretch, three-body angle bending, and four-body proper and improper torsions) and nonbonding terms (Lennard-Jones and electrostatics) to the energy flow separately.

We have carried out such an analysis for the nonzero contribution atoms of the heme iron. Table 4 shows the bonding and nonbonding contribution atoms of the heme iron 1 fs after oxidation of the protein for the energy flow calculations starting from the 250-ps snapshot of the ferrocytochrome *c* trajectory. Table 5 is similar, except that the 150-ps snapshot was used. From Tables 4 and 5, one can see that the bonding oxidation-sensitive atoms of the heme iron were the same in the two cases, whereas the nonbonding oxidation-sensitive (NBOS) atoms were slightly different. For example, the carbonyl group of LYS79 were NBOS atoms of the heme iron in the former, but not in the latter case. On the other hand, the carbonyl carbon of HIS18, the carbonyl oxygen of HIS18, the carbonyl carbon of ILE81, and the carbonyl oxygen of ILE81 were NBOS atoms of the heme iron in the latter, but not in the former case. Therefore, atoms that are separated from each other by fewer than four bonds may be more likely to make contributions to each other's energy flow. However, this may not be the case for atoms that are not bonded together, even when they are not too far apart.

CONCLUSIONS

A method for studying energy flow in proteins has been introduced. Its utility was first illustrated by applying it to study a cluster of 13 argon atoms arranged in icosahedral geometry. It was found that collective motions of the clusters facilitated energy transfer in this cluster. The method for studying energy flow was then applied to the study of a more complicated protein molecule, tuna cytochrome *c*. The pattern of energy flow after the heme group of the protein was oxidized was quite complex. There was no simple correlation between the time needed for an atom to feel the effect of the oxidation of the protein and the distance of the atom from the oxidation site of the protein. Some atoms far away from the heme iron were found to respond quickly to the oxidation of the heme. Some of these atoms sensed the effects of the oxidation directly through long-range electrostatic interactions with atoms associated with the oxidation site of the protein. Others detected the oxidation effects indirectly by interacting with atoms that communicated directly with the oxidation site through short-range, long-range, bonded, or nonbonded interactions. Overall, it took no more than ~40 fs before all of the atoms of the protein felt the effects of the oxidation of the heme.

For tuna cytochrome *c*, energy dissipated more efficiently along the axial direction of the heme. This is due to the efficient through-bond mechanism involving residues His^{18} and Met^{80} that are covalently bonded to the heme iron. The propionate groups of the heme also provided an efficient mechanism for directing energy away from the heme after heme oxidation. This was due to the favorable electrostatic interactions between the charged carboxylates of the propionates and the iron site that underwent a change in oxidation state after electron transfer.

This research was supported in part by the National Institutes of Health and the National Science Foundation. Prof. Wilfred van Gunsteren generously provided the GROMOS program.

REFERENCES

Berendsen, H. J. C., J. R. Grigera, and T. P. Straatsma. 1987. The missing term in effective pair potentials. *J. Phy. Chem.* 91:6269–6271.

Berendsen, H. J. C., J. P. M. Postma, W. F. van Gunsteren, A. DiNola, and J. R. Haak. 1984. Molecular dynamics with coupling to an external bath. *J. Chem. Phys.* 81:3684–3690.

Berghuis, A. M., and G. D. Brayer. 1992. Oxidation state-dependent conformational changes in cytochrome *c*. *J. Mol. Biol.* 223:959–976.

McCammon, J. A., and S. C. Harvey. 1987. Dynamics of Proteins and Nucleic Acids. Cambridge University Press, Cambridge.

McQuarrie, D. A. 1976. Statistical Mechanics. Harper and Row, New York.

Ryckaert, J. P., G. Ciccotti, and H. J. C. Berendsen. 1977. Numerical integration of the Cartesian equations of motion of a system with constraints: molecular dynamics of *n*-alkanes. *J. Comput. Phys.* 23: 327–341.

Schwieters, C. D., and H. Rabitz. 1994. Display of the flow of energy in molecules. *J. Comp. Chem.* 15:80–89.

Takano, T., and R. E. Dickerson. 1981. Conformation change of cytochrome *c*: ferrocytochrome *c* structure refined at 1.5 Å resolution. *J. Mol. Biol.* 153:79–94.

van Gunsteren, W. F., and H. J. C. Berendsen. 1987. GROMOS. University of Groningen, Groningen, The Netherlands.

Wong, C. F., C. Zheng, J. Shen, J. A. McCammon, and P. G. Wolynes. 1993. Cytochrome *c*: a molecular proving ground for computer simulations. *J. Phys. Chem.* 97:3100–3110.